Biomaterials 236 (2020) 119802

Contents lists available at ScienceDirect

Biomaterials

journal homepage: www.elsevier.com/locate/biomaterials

Three-dimensional self-assembling nanofiber matrix rejuvenates aged/degenerative human tendon stem/progenitor cells

Heyong Yin[a,b,1], Franziska Strunz[a,1], Zexing Yan[a], Jiaju Lu[c], Christoph Brochhausen[d], Stefanie Kiderlen[e,f], Hauke Clausen-Schaumann[e,f], Xiumei Wang[c], Manuela E. Gomes[g], Volker Alt[a], Denitsa Docheva[a,*]

[a] Experimental Trauma Surgery, Department of Trauma Surgery, University Regensburg Medical Centre, Regensburg, Germany
[b] Department of Orthopedics, Beijing Friendship Hospital, Capital Medical University, Beijing, China
[c] State Key Laboratory of New Ceramics and Fine Processing, School of Materials Science and Engineering, Tsinghua University, Beijing, China
[d] Institute of Pathology, University Regensburg Medical Centre, Regensburg, Germany
[e] Center for Applied Tissue Engineering and Regenerative Medicine, Munich University of Applied Sciences, Munich, Germany
[f] Center for NanoScience, Ludwig-Maximilians-University, Munich, Germany
[g] 3B's Research Group, I3Bs-Research Institute on Biomaterials, Biodegradables and Biomimetics, University of Minho, Headquarters of the European Institute of Excellence on Tissue Engineering and Regenerative Medicine, Guimarães, Portugal

ARTICLE INFO

Keywords:
Hydrogel
3D microenvironment
Stem/progenitor cell
Cell aging
Rejuvenation

ABSTRACT

The poor healing capacity of tendons is known to worsen in the elderly. During tendon aging and degeneration, endogenous human tendon stem/progenitor cells (hTSPCs) experience profound pathological changes. Here, we explored a rejuvenation strategy for hTSPCs derived from aged/degenerated Achilles tendons (A-TSPCs) by providing three-dimensional (3D) nanofiber hydrogels and comparing them to young/healthy TSPCs (Y-TSPCs). RADA peptide hydrogel has a self-assembling ability, forms a nanofibrous 3D niche and can be further functionalized by adding RGD motifs. Cell survival, apoptosis, and proliferation assays demonstrated that RADA and RADA/RGD hydrogels support A-TSPCs in a comparable manner to Y-TSPCs. Moreover, they rejuvenated A-TSPCs to a phenotype similar to that of Y-TSPCs, as evidenced by restored cell morphology and cytoskeletal architecture. Transmission electron, confocal laser scanning and atomic force microscopies demonstrated comparable ultrastructure, surface roughness and elastic modulus of A- and Y-TSPC-loaded hydrogels. Lastly, quantitative PCR revealed similar expression profiles, as well a significant upregulation of genes related to tenogenesis and multipotency. Taken together, the RADA-based hydrogels exert a rejuvenating effect by recapitulating *in vitro* specific features of the natural microenvironment of human TSPCs, which strongly indicates their potential to direct cell behaviour and overcome the challenge of cell aging and degeneration in tendon repair.

1. Introduction

Tendons are hierarchically organized, dense connective tissues integrating the musculoskeletal system, withstanding tension and allowing proper movement of the body [1,2]. Mature tendons are hypocellular with 90–95% of the identified cells being tenoblasts and terminally differentiated tenocytes [1,3,4]. In addition, tendons harbour a unique cell population identified as tendon stem/progenitor cells (TSPCs) that are clonogenic, self-renewable, and multipotent [5], and are considered important for tissue homeostasis and during times of repair [6–8]. Therefore, TSPCs combined with biomaterials and biological cues are a promising target for augmentation of tendon healing [9,10].

Tendons have a high risk of injury during accidents and intensive

* Corresponding author. Director of Experimental Trauma Surgery, Department of Trauma Surgery, University Regensburg Medical Centre, Franz-Josef-Strauss-Allee 11, 93053, Regensburg, Germany.
E-mail addresses: heyong.yin@ukr.de (H. Yin), franziska.strunz@stud.uni-regensburg.de (F. Strunz), zexing.yan@ukr.de (Z. Yan), lujj13@mail.tsinghua.edu.cn (J. Lu), christoph.brochhausen@ukr.de (C. Brochhausen), stefanie.kiderlen@hm.edu (S. Kiderlen), hauke.clausen-schaumann@hm.edu (H. Clausen-Schaumann), wxm@mail.tsinghua.edu.cn (X. Wang), megomes@i3bs.uminho.pt (M.E. Gomes), volker.alt@ukr.de (V. Alt), denitsa.docheva@ukr.de (D. Docheva).
[1] The authors contributed equally to this work.

https://doi.org/10.1016/j.biomaterials.2020.119802
Received 29 July 2019; Received in revised form 14 January 2020; Accepted 18 January 2020
Available online 21 January 2020

sports, as well as due to age-related tissue degeneration [11,12]. In addition, tendons have a poor healing capacity that even worsens in the elderly because of an exhaustion of the endogenous TSPC pool coupled with impaired cellular functions [7,13]. Thus, a main challenge for stem cell-based therapies is various changes accumulating in the therapeutic cells during organismal and tissue aging. These include alterations at the epigenetic, genomic, transcriptomic, and proteomic levels resulting in declined stem cell functionality and repair capacity [7,8,14,15].

We have previously established and characterized in detail two clinically relevant cell types, TSPC isolated from aged/degenerated human Achilles tendon biopsies (A-TSPCs) and TSPC isolated from Achilles tendon biopsies of young/healthy donors [7,14,15]. In comparison to Y-TSPCs, A-TSPCs exhibited complex phenotypic changes comprising of profound self-renewal and clonogenic deficits, altered cell morphology (significantly larger cell area with polygonal shape), abnormal cytoskeletal architecture (increase in F-actin content) , slower actin turnover and overall cell stiffening (higher Young's modulus), premature entry into senescence, significantly reduced migratory potential and distinct transcriptional shift [7,14,15]. Hence, a rejuvenation or appropriate support of aged stem/progenitor cells is crucial to restore normal cellular functions and improve tissue repair outcome.

The ECM is a three-dimensional (3D) environment containing macromolecular components organized in fibrillar structures with unique biophysical and biochemical attributes that plays a key role in governing cell functions in native tissues [16]. Li et al. have reported that extracellular matrix (ECM) deposited by fetal synovium-derived stem cells (SDSCs) exerts rejuvenating effects onto adult SDSCs [17]. Cosgrove et al. have demonstrated another powerful restorative strategy for aged skeletal muscle stem cells composed of soft hydrogel substrates encapsulating p38α/β inhibitor [18]. These new insights indicate that a specific targeting of the ECM microenvironment of the cells may be one way to develop novel rejuvenation schemes for stem/progenitor cell functional improvement.

The self-assembling peptide RADA, made of the natural amino acids arginine, alanine, and aspartic acid (Ac-$(RADA)_4$-$CONH_2$), can undergo spontaneous assembly into a nanofiber hydrogel with 10 nm fiber diameter, 5–200 nm pore size, and > 99% water content [19]. Importantly, the self-assembled nanofibers are much thinner than cells, thus it is believed that the peptide nanofibers surround cells in a manner similar to the natural 3D ECM. Hence, the nanofiber hydrogels have distinct advantages in comparison to many processed synthetic polymers consisting of microfibers bigger than 10 μm in diameter, which exceed native protein fibers. For example, in tendon, the collagen fibrils to which cells attach, are in the range of 50–200 nm [20]. Thus, cells bound to microfibers are still in a 2D environment with a curvature dependent upon the diameter of the microfibers [19]. RADA-based 3D culture models have been tested with various cell types for tissue engineering approaches [21–24]. Furthermore, RADA can be functionalized by directly adding RGD (arginine, glycine and aspartate) motif that is an integrin-binding domain (found in the ECM proteins fibronectin, vitronectin and laminin) mediating cell attachment [19]. Importantly, the functionalized RADA/RGD peptide hydrogel exhibits a similar potential to form a nanofiber 3D structure, as its a non-functionalized version [19].

Using RADA and RADA/RGD hydrogels, we explored in the current study how their 3D microenvironment will affect A-TSPCs biological behaviour. Based on the above, in the current study, we hypothesize that these nanofiber hydrogels can rejuvenate A-TSPCs to a younger phenotype by providing the nanoscale fibrous structure mimicking the natural tendon ECM. Human Y- and A-TSPCs were cultivated in both types of hydrogel, and their cell survival, proliferation, apoptosis, cell morphology, F-actin organization, cell alignment and gene expression profiles were evaluated. In addition, confocal laser scanning microscopy (CLSM) was employed to visualize the topography and analyse the surface roughness of un- and cell-loaded nanofiber hydrogels, transmission electron microscopy (TEM) was used to study the ultrastructure of the cells and their interactions with the RADA and RADA/RGD nanofibers, and lastly, an indentation type of atomic force microscopy (AFM) was performed to assess the elastic moduli of the TSPC-3D hydrogel cultures.

2. Materials and methods

2.1. Human cell culture

Human TSPCs were isolated from non-ruptured young/healthy (Y-TSPCS) (n = 4, average 28 ± 5 years) or aged/degenerative Achilles tendon biopsies (A-TSPCs) (n = 12, average 63 ± 14 years) as described and characterized in detail by Kohler et al. [7]. From the primary donor cohort, three donor Y-TSPCs (Y1-, Y2-, Y3-TSPC) and three donor A-TSPCs (A1-, A2-, A3-TSPC) were employed for detailed transcriptome analyses and pharmacological rejuvenation studies [7,15]. Therefore, in this investigation, we used the same six donor cells. All the donors were male. The cell isolation protocol was carried out in accordance to the Ethical Grant No. 166-08 of the Ethical Commission of the LMU Medical Faculty. Briefly, Achilles tendon tissue was minced and digested with 0.15% collagenase II (Worthington, Lakewood, NJ, USA) overnight at 37 °C, filtered with a nylon mesh (pore size 100 μm), and centrifuged at 500 g for 10 min. Thereafter, cell pellets were resuspended in TSPC culture medium consisting of DMEM/Ham'sF-12 (Biochrom, Berlin, Germany) supplemented with stabile glutamine (Sigma-Aldrich, Munich, Germany), 10% FBS (PAN Biotech, Aidenbach, Germany), 1% penicillin/streptomycin (Sigma-Aldrich), 1% MEM (Biochrom, Berlin, Germany), and 1% L-ascorbic acid-2-phosphate solution (Sigma-Aldrich). Based on the published growth kinetics [7], Y-TSPC and A-TSPC were used up to passage 12 (p12) and 7 (p7), respectively.

To confirm the multipotency of the cells used in the study, Y-TSPC (n = 3, p12) and A-TSPC (n = 3, p7) were stimulated towards trilineages in 2D and 3D (RADA group) culture conditions for 21 days. For chondrogenic lineage, per donor 2×10^5 cells/donor were pelleted (10 pellets/donor) as classical chondorgenic pellet culture and 2×10^5 cells were mix 60 μl RADA gel (10 gels/donor) and casted. One half of the pellets and gels were supplemented for 21 days with stimulation media (DMEM high glucose serum-free, 10 ng/ml TGFβ1, 100 nM dexamethasone, 50 ng/ml ascorbic acid, 1 mM sodium pyruvate and (all Sigma-Aldrich), 1% ITS (PAN). Media was changed thrice/week. In parallel, the other half was kept in control media without TGFβ1. At day 21, pellets and gels were collected, fixed 4% paraformaldehyde (PFA), cryo-protected and cut (10 μm thickness) and stained with 5% 1,9-dimethylmethylene blue (DMMB). For adipogenic, for 2D $8 \times 10^3/cm^2$ were plated in 12-well dishes (6 wells/donor) and 4×10^3 were plated onto 60 μl RADA gel (6 gels/donor) and half were given DMEM high glucose, 10% FBS, 1 μM dexamethasone, 0.2 mM indomethacin, 0.1 mg/ml insulin and 1 mM IBMX osteogenic (all Sigma-Aldrich) with media being change twice/week. Unstimulated controls were given just DMEM high glucose and 10% FBS. To visualize adipogenesis, 2D cultures were fixed with 10% formaldehyde, washed with 60% isopropanol and stained with 0.3% Oil Red O solution (10 min at RT) labelling adipocytes in red color. Since empty RADA hydrogels trap the Oil Red O dye, hence giving false positive signal, the adipogenic differentiation in 3D was confirmed by detecting cell lipid droplets by phase-contrast microscopy. Last, for osteogenic differentiation in 2D $4 \times 10^3/cm^2$ were plated in 12-well dishes (6 wells/donor) and 2×10^3 were plated onto 60 μl RADA gel (6 gels/donor) and half were given DMEM high glucose, 10% FBS, 0.1 μM dexamethasone, 1 mM β-glycerophosphate and 50 μM ascorbic acid (all Sigma-Aldrich) with media being change twice/week. Unstimulated controls were given just DMEM high glucose and 10% FBS. For 2D, cells were fixed with 10% formaldehyde, washed and incubated with 40 mM Alizarin Red for 30 min at RT, washed 4 times and imaged. Calcified

matrix is colored in red. Similar to Oil Red O, Alizarin Red also gives false positive signal in empty RADA. Therefore for the 3D group, the supernatants of unstimulated and stimulated samples (collected in the 3rd week, pool of 2 media changes) were collected and measured for alkaline phosphatase (ALP) activity by incubating for 2 h with p-N-phenol phosphate substrate (Sigma-Aldrich). Fluorometric measurements were done at 405 nm using Tecan instrument (Genios FL Fluorescence Plate Reader, Tecan, Switzerland).

2.2. Preparation of self-assembling peptide hydrogels

Pure and sterile RADA peptide with a concentration of 1% (w/v) was commercially purchased from Corning (Corning PuraMatrix, New York, USA). The RGD motif was added by direct extension to RADA C-terminus to form the designer RADA-RGD peptide (Ac-$(RADA)_4$ -GG-RGDS-$CONH_2$), which was custom-synthesized with a stock concentration of 1% (w/v) and sterilized by China Peptides (Shanghai, China). To prepare a working concentration, 1% RADA-RGD peptide solution was mixed 1:1 (v/v) with 1% pure RADA peptide solution to prepare to the functionalized RADA/RGD peptide. Both the RADA and RADA/RGD peptides undergo spontaneous assembly and gelation into hydrogels with nanofiber structure in the presence of a physiological salt solution.

2.3. Three-dimensional culture of TSPCs in the nanofiber hydrogels

For 3D culture of TSPCs in RADA or RADA/RGD nanofiber hydrogels, 6×10^4 Y- or A-TSPCs were encapsulated in 60 μl hydrogel solution. Briefly, TSPCs were trypsinized, spun down at 1000 g for 5 min, re-suspended in 20 μl sterile 10% sucrose solution, mixed thoroughly with 40 μl RADA or RADA/RGD peptide solution, then 60 μl cell/peptide mixture was pipetted into a sterile cylindrical mould (5 mm in diameter and 5 mm in height) and covered with 100 μl culture medium to trigger the gelation. After 10 min incubation at 37 °C, hydrogels encapsulating TSPCs were punched out and were cultivated free floating in culture medium in 24-well dishes and used for all follow up experiments, apart from staining and RNA isolation experiments. Alternatively, nanofiber hydrogels were prepared using cell culture inserts with a pore size of 0.4 μm (Greiner, Frickenhausen, Germany) in 24 well plates. Briefly, 60 μl of cell (6×10^4 cells)/peptide suspension was pipetted into the inserts and then 100 μl medium were added on top. The bottoms of the 24 well plates were filled with culture medium up to 800 μl and after 10 min incubation at 37 °C, additional 200 μl medium were added into the inserts. Medium changes were performed every 2 days.

For analysis of gel diameter change, cell-loaded RADA and RADA/RGD hydrogels (n = 3 gels for Y3-TSPC) were photographed and measured at d1 and d7 of culture.

2.4. TSPCs survival, apoptosis, and proliferation in the nanofiber hydrogels

Live/dead staining was performed at day 1, 3, and 7 to assess cell survival within both nanofiber hydrogels. Briefly, the cell-loaded hydrogels (n = 3 Y-TSPC and n = 3 A-TSPC donors, 2 gels/donor) were twice washed with PBS and then stained with 5 μg/ml calcein AM (labelling live cells) and 5 μg/ml ethidium homodimer-1 (labelling dead cells) (Molecular probes, Eugene, Oregon, USA) at 37 °C for 40 min. After washing, the hydrogels were transferred to a glass slide and covered with fluorescent-protective media (Mowiol) for imaging. In short, the cell-loaded hydrogels (n = 3 Y-TSPC and n = 3 A-TSPC donors, 2 gels/donor) were washed with PBS, incubated in 10 μg/ml JC-1 dye (Molecular Probes) at 37 °C for 40 min, rinsed thrice with PBS, transferred to a glass slide, covered with Mowiol and subjected to imaging. For the live/dead and JC-1 stainings, multiple fluorescence images were taken with an Olympus XC10 camera mounted on an Olympus BX61 fluorescence microscope (Olympus, Shinjuku, Japan) and z-stacking was performed with up to 10 images per sample by using Adobe Photoshop CS v6 (Adobe Systems, San Jose, CA). To quantify the number of live and dead cells: 1) 1 image/gel (6 images/donor group) were taken with 20× magnification; 2) in each image, the number of green and red cells was manually counted and expressed as % of the green from the total cell number. To specifically monitor occurrence of cell apoptosis, fluorescent JC-1 staining (mitochondrial membrane potential assay) was conducted within both types of hydrogels at day 7. Early stage programmed cell death is associated with changes in the mitochondria membrane potential. JC-1 dye possesses potential-dependent accumulation property in mitochondria in living cells (labelled in red) and if membrane potential is lost, the same dye experiences a fluorescence emission shift to green, thus directly indicating apoptotic cells. Resazurin assay was carried out to evaluate cell metabolic/proliferative activity within the hydrogels over culture time of 6 h, 1, 3, and 7 days. The cell-loaded hydrogels (n = 3 Y-TSPC and n = 3 A-TSPC donors, 2 gels/donor) were incubated in 100 μl 10% (v/v) Resazurin (Sigma-Aldrich) in culture medium at 37 °C for 3 h. Afterwards, 60 μl supernatant was collected and photometrically measured with 545 nm excitation filter and 590 nm emission filter (Genios FL Fluorescence Plate Reader, Tecan, Switzerland). In addition, as 2D control, 1×10^3 TSPCs/well were cultured in 12-well dishes (Y-TSPCs, n = 3, p12 and A-TSPCs, n = 3, p7; 4 wells/donor) and 1 ml 10% Resazurin solution was given at 1, 3 and 7 days of culture for 1 h. Thereafter, 100 μl supernatant was collected and measured as described above.

2.5. TSPCs morphology, F-actin organization and alignment in the nanofiber hydrogels

F-actin staining was performed to visualize cell morphology at day 7. For this, cell-loaded RADA and RADA/RGD hydrogels (n = 3 Y-TSPC and n = 3 A-TSPC donors, 2 gels/donor) were fixed in 4% PFA (paraformaldehyde at room temperature (RT) for 20 min, rinsed with PBS, permeabilized with 0.2% Triton X-100/PBS for 10 min and then blocked with 1% BSA in PBS at RT for 1 h. In addition, both types of TSPCs (Y-TSPCs, n = 3, p12 and A-TSPCs, n = 3, p7) were in 2D as well as in 3D collagen I hydrogels as described previously by us [25] for 3 days. Next, phalloidin-AF488 or AF594 (Life technologies, Carlsbad, California, USA; 1:400 in blocking solution) was applied at RT for 120 min. DAPI was used for nuclear counter-staining (Sigma-Aldrich; 1:10,000 in PBS) and applied at RT for 60 min. Multiple fluorescence images were taken as described above to monitor cell shape and cytoskeletal architecture. For analysis of cell aspect ratio (width/length) and cell area, selected images (for each cell type, n = 3 donors, 2 gels/donor, 45 cells/group) were evaluated with ImageJ-Pro Plus v6.0 software (National Institutes of Health, Bethesda, MD, USA) using "count and measure objects" tool. Cell aspect ratio (cell width divided by cell length) close to 1, indicates a cell with a round shape, whilst near to 0, indicates an elongated cell shape [25]. The TSPC alignment within the RADA and RADA/RGD nanofiber hydrogels was investigated using bright-field optical images taken with an Olympus XC10 camera mounted on an Olympus BX61 fluorescence microscope of semi-thin (0.8 μm) sections of cell-loaded hydrogels that were pre-stained with 1% toluidine blue and basic fuchsin at RT for 1–2 min. For each cell type, 3 donors (1 image/donor) were analyzed. The images were first converted to 8-bit grayscale and two-dimensional Fast Fourier transformation (2D-FFT) was performed with ImageJ software according to Tognato et al. [26]. The resulting 'frequency' domain images were tilted 90° to invert the intrinsic rotation due to the 2D-FFT. The pixel intensities were summed along the radius for each angle of the circular projection and plotted as a function of the corresponding angle of acquisition using "oval profile" plugin. All alignment plots were normalized to a straight baseline value of 0 and plotted in arbitrary units.

2.6. Confocal laser scanning microscopy (CLSM)

Surface topography RADA and RADA/RGD nanofiber hydrogels were analyzed by CLSM. At day 7, empty and cell-loaded hydrogels were collected, rinsed with PBS and incubated overnight in 4% paraformaldehyde, 4% glutaraldehyde, 15% saturated picric acid solution, and 0.1% Triton X-100. Next, after brief washing, the samples were stained in 0.1% Dimethylmethylene Blue (DMMB) solution for 40 min, dehydrated with an isopropanol gradient (55%, 70%, 80%, 90%, 95%, and 100%; each 40 min), treated with 100% tertiary butanol overnight, and then subjected to vacuum drying. Sample scanning was performed using an Olympus LEXT OLS4000 laser microscope with a wavelength of 405 nm and a threshold wavelength of 80 nm. Hydrogel topography was imaged at 426× and 1069× magnification. Surface roughness is the average absolute value of the height deviation from the arithmetical mean plane. The CLSM examination has been performed with three Y-TSPC and three A-TSPC donors, each donor represented with 1 RADA and RADA/RGD gel. Each gel sample was analyzed at three different points.

2.7. Transmission electron microscopy (TEM)

TEM was used to study the ultrastructure of the cells and their interactions with the RADA and RADA/RGD nanofibers at day 7. Hydrogels were fixed in Karnovsky (0.1 M cacodylate-buffer with 2.5% glutaraldehyde and 2% paraformaldehyde), enclosed in 4% low-melting agarose, post-fixed in 1% osmium tetroxide (pH 7.3), dehydrated in graded ethanol, and embedded in the EMbed-812 epoxy resin (all reagents purchased from Science Services, Munich, Germany). After 48 h heat polymerization at 60 °C, semi-thin sections (0.8 μm) were cut. The slides were stained with 1% toluidine blue and basic fuchsin. Ultrathin sections (0.08 μm) were cut with a diamond knife on a Reichert Ultracut-S ultramicrotome (Leica, Bensheim, Germany). Sections were mounted on grids and double stained with aqueous 2% uranyl acetate and lead citrate solutions (each for 10 min). The ultrathin sections were examined in a LEO912AB electron microscope (Zeiss, Oberkochen, Germany) operating at 100 kV. Findings were documented with a side-mounted 2 k x 2 k-CCD-camera (TRS, Moorenweis, Germany). The TEM examination was performed on three Y-TSPC and three A-TSPC donors, (1 RADA and 1 RADA/RGD gel/donor).

2.8. RNA isolation, cDNA synthesis, and quantitative PCR

Total RNA from TSPCs (n = 3 Y-TSPC and n = 3 A-TSPC donors, 3 gels/donor) cultured in the 3D hydrogels as well as in 2D monolayer was extracted at day 3 using Qiagen RNeasy Mini kit (Qiagen, Hilden, Germany) according to the manufacturer's instructions. Genomic DNA was eliminated with gDNA eliminator solution (RNeasyPlus Universal Mini Kit). The RNA purity was checked with NanoDrop (ThermoScientific, Waltham, MA, USA; absorbance ratios of 260/280 nm were in the range of 1.8–2.2), whilst RNA integrity was confirmed with Agilent RNA 6000 Nano Kit (Agilent Technologies, Santa Clara, California, USA). Four parallel cDNA synthesis reactions (total volume of 80 μl; RNA input 0.2–1 μg) per donor were performed with a Transcriptor First-Strand cDNA Synthesis Kit (Roche Diagnostics, Mannheim, Germany). Quantitative PCR for 48 different genes and 2 reference genes (Table S1) was performed using RealTime PCR Ready Custom design plates with format 96-well/32+ according to the manufacturer's instructions (Roche, Penzberg, Germany). Briefly, qPCR reactions were pipetted on ice and each well contained 10 μL LightCycler 480 probes master mix (Roche), 1 μL cDNA and 9 μL PCR grade water. Plates were subsequently sealed and centrifuged down at 2000 rpm for 15 s. Six experimental groups each with 3 donors/group were evaluated (Y-TSPC 2D, A-TSPC 2D, Y-TSPC RADA, A-TSPC RADA, Y-TSPC RADA/RGD, and A-TSPC RADA/RGD). Crossing points for each sample were determined by the second derivative maximum method. The reference gene GAPDH was used for normalization. Fold change was calculated by the $2^{-\Delta\Delta Ct}$ method, where $\Delta Ct = Ct_{target} - Ct_{GAPDH}$ and $\Delta\Delta Ct = \Delta Ct_{\text{3D TSPCs (test)}} - \Delta Ct_{\text{2D TSPCs (calibrator)}}$. Delta Ct values of all the genes for the 6 different groups were plotted in Table S1. Fold change and statistical significance between the six groups were calculated with the Bio-Rad CFX Maestro software (Bio-Rad Laboratories, GmbH, Munich, Germany). Only genes with significant change in expression were plotted in bar graphs.

2.9. Force indentation atomic force microscopy (FI-AFM)

For FI-AFM cell-loaded RADA and RADA/RGD hydrogels at day 7 were fixed in 95% ethanol and 5% glacial acetic acid at 4 °C for 1 h for morphology preservation, then submitted to 70% overnight and rehydrated as follows: 60% ethanol at RT for 1 h, followed by 50% ethanol at RT overnight, and in PBS at RT for 1 h. During the last 5 min of PBS incubation, Hoechst H6024 nucleus staining (Sigma-Aldrich) was performed for cell identification. Subsequently, the hydrogels were embedded in Tissue-tek (Sakura, Torrance, CA, USA) and 100 μm thick cryo-sections were cut using a CM1950 cryotome (Leica Biosystems, Bensheim, Germany) [27]. Fixing and embedding increases samples stiffness which also allows higher forces to be applied during AFM measurement, which together with tip sharpness and pixel density significantly increases image resolution [28]. In addition, the elevated stiffness through fixation ensures improved reproducibility between data sets [28]. Importantly, ethanol-based fixation allows good re-hydration that is in contrast to formalin-based fixation and second, all of the samples were prepared and fixed the same way. The FI-AFM, NanoWizard (JPK Instruments, Berlin, Germany) equipped with a 100 μm × 100 μm x 15 μm piezo scanner, was mounted on an inverted optical microscope (Axiovert 200, Carl Zeiss, Oberkochen, Germany). FI-AFM indentation experiments were carried out in PBS at RT using MLCT cantilevers (Bruker) with a nominal spring constant of 0.1 N/m. Arrays of 25 × 25 force-distance curves were recorded in a 3 μm × 3 μm scan area, at a z-piezo velocity of 2 μm/s. The indentation force was limited to 5 nN and the Young's modulus was derived from the indentation part of the curves, as described previously [27,29]. The actual cantilever force constant was determined for each cantilever individually, using the thermal noise method [30]. All data analysis was performed with the JPK software v. 6.0.69. Three Y-TSPC and three A-TSPC donors (1 gel/donor) were investigated. Per gel, 625 force curves were analyzed for estimation of Young's modulus and plotted in graphs. In total, for Y-TSPC RADA, A-TSPC RADA, Y-TSPC RADA/RGD, and A-TSPC RADA/RGD groups, 1875 force curves/group were analyzed.

2.10. Collagen type I protein analysis

For collagen type I protein analysis, 2×10^5 cells were mix 60 μl RADA gel (Y-TSPCs, n = 3, p12 and A-TSPCs, n = 3, p7; 3 gels/donor), casted, cultivated in 10 ng/ml TGFβ1-suplimented culture media, collected, fixed 4% PFA, cryo-protected and cut (10 μm thickness). Cryosections were treated for antigen retrieval with 1% pepsin for 15 min at RT blocked by 1% bovine serum albumin (BSA) for 1 h, and incubated with primary anti-collagen type I antibody (Sigma-Aldrich, Cat. Nr. C2456, 1:200 dilution) overnight at 4 °C. Next day, anti-mouse FITC secondary antibody (Sigma-Aldrich) was applied for 1 h at RT, and last DAPI counterstaining was done for 5 min. Fluorescent images were acquired with an Olympus XC10 camera on an Olympus BX61 fluorescence microscope and quantitative image analysis was carried out as follows: 1) 1 image/gel (9 images/donor group) were taken with 20× magnification; 2) the fluorescent images were converted in gray scale; 3) for each image “set measurments” for image area, integrated density and mean gray value was selected from the analysis menu; 3) the total cryosection fluorescence was exported and expressed as mean fluorescent intensity arbitrary units (A.U.).

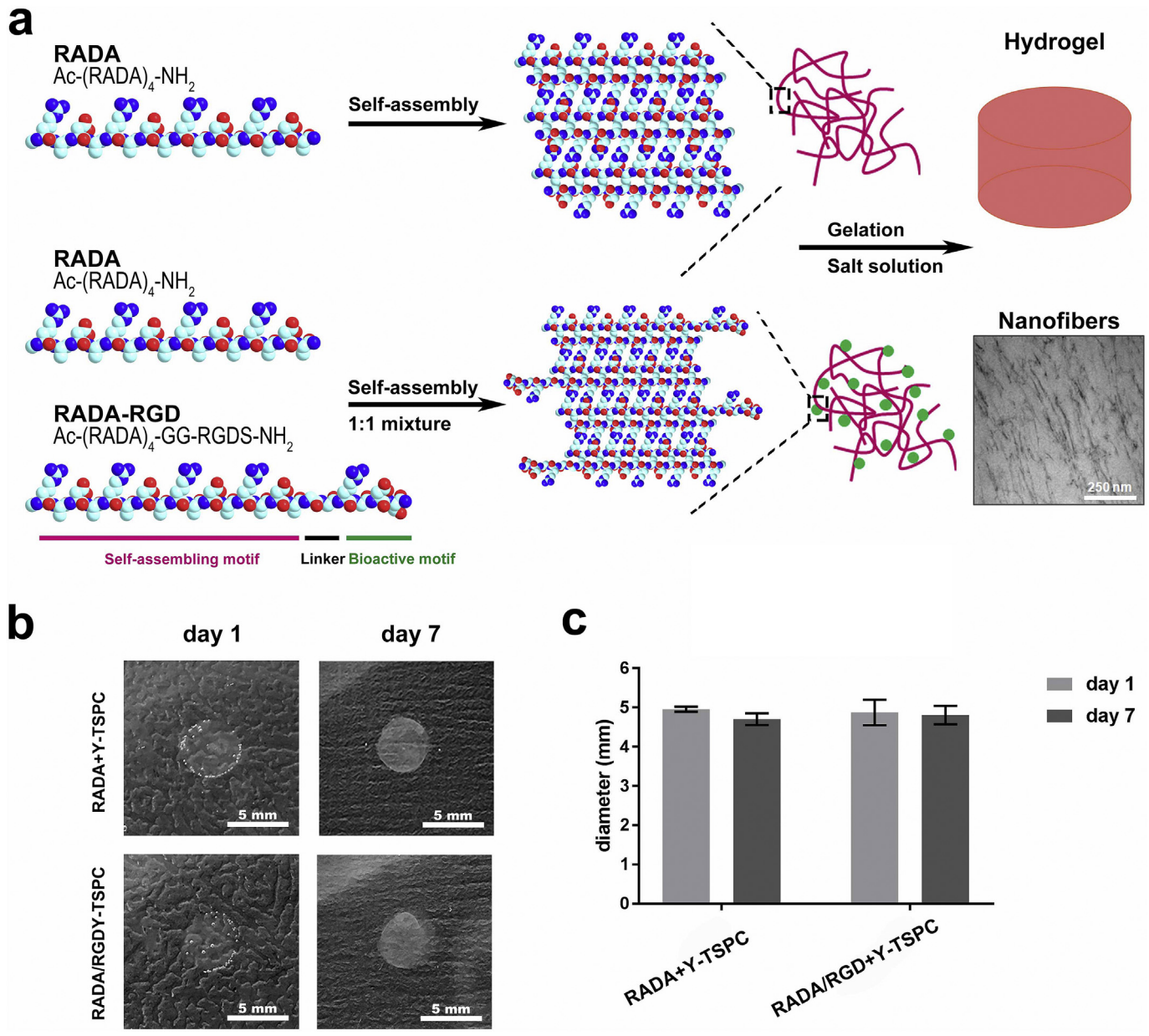

Fig. 1. RADA and RADA/RGD preparation and stability. (a) Schematic diagram depicting the molecular self-assembly and hydrogel formation. (b) Representative images of cell-loaded hydrogels at day 1 and 7 of culture (Y3-TSPCs). (c) Diameter changes of TSPC-loaded peptide hydrogels over time (n = 3 Y-TSPCs).

2.11. Statistical analysis

Data in graphs is presented as mean ± standard deviation. Biological and technical repeats are given for each method above. Statistical differences between two groups (Fig. 6a and b, 3D vs 2D) were determined using unpaired Student's t-test with GraphPad Prism v7 software (GraphPad Software Inc, CA, USA). ANOVA was used to determine statistical significant between multiple groups (Fig. 1c, Fig. 2b, Fig. 3b, Fig. 4 c and Fig. 7b). Differences were considered statistically significant when p-values < 0.05 (*) and < 0.01 (**).

3. Results

3.1. Validation in 2D and three-lineage differentiation of Y- and A-TSPCs in 2D and 3D

We first validated the phenotype differences between Y- and A-TSPCs in 2D culture condition (Fig. S1Fig. S1). Phase-contrast imaging confirmed that Y-TSPCs convey a classical spindle-like cell shapes, while A-TSPCs exhibit a polygonal cell morphologies with larger cell areas (Fig. S1). Actin visualization confirmed the morphological differences, as well as demonstrating that A-TSPCs have more actin stress fibers and higher actin content than Y-TSPCs (Fig. S1). This was also true when the cells were cultivated in collagen I hydrogels (Fig. S1d). In addition, Resazurin assay showed that the aged cells have significantly declined self-renewal ability in 2D (Fig. S1). These results are consistent with our previous findings [7], thus confirming that the phenotypic abnormalities in aged cells persist in 2D. In addition, Y- and A-TSPCs were successfully induced into chondrogenic, adipogenic and osteogenic differentiations in both 2D (as previously reported in Kohler et al., 2013 [7]), as well as in the 3D hydrogel cultures (Fig. S2), proving that the cells retain their multipotency.

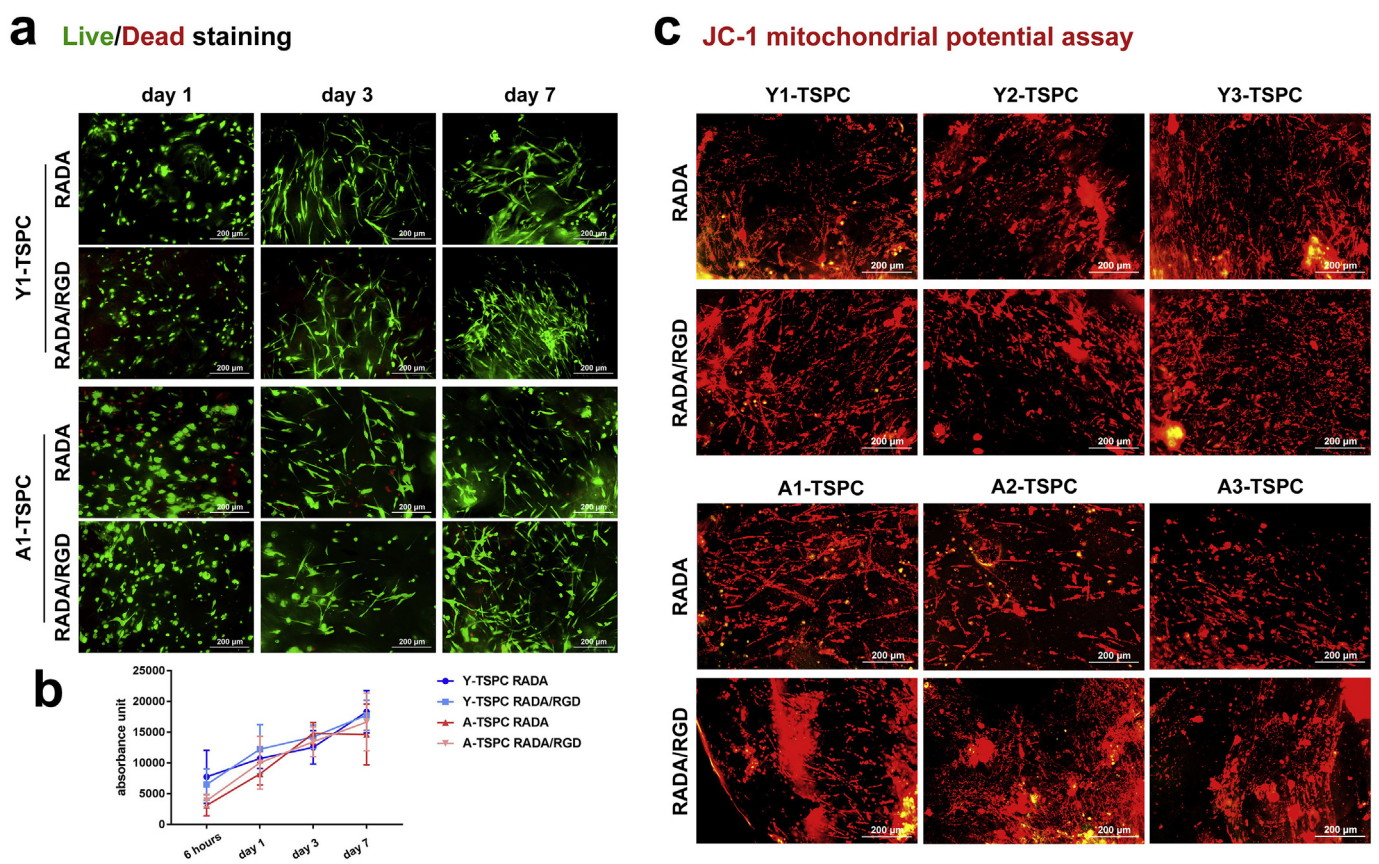

Fig. 2. Investigation of cell survival, proliferation and apoptosis within the RADA and RADA/RGD nanofiber hydrogels. (a) Representative live/dead staining of Y1- and A1-TSPC-loaded at day 1, 3 and 7 (for Y2-, Y3-, A2-and A3-TSPCs refer to Fig. S4). Live cells are labelled in green; dead cells in red. (b) Resazurin assay for cell metabolic/proliferative activity of Y-TSPCs (n = 3) and A-TSPCs (n = 3) cultured in RADA and RADA/RGD nanofiber hydrogels carried out 6, 24, 72 and 168 h. (c) Representative JC-1 fluorescent photomicrographs of all donor cells. Live cells are labelled in red; apoptotic cells in green. All experiments were carried out with n = 3 Y-TSPC and n = 3 A-TSPC donors, 2 gels/donor.

3.2. RADA and RADA/RGD nanofiber hydrogels self-assemble and when loaded with cells remain stable in culture

Fig. 1a describes the the RADA and RADA/RGD formulations, as well as the self-assembly process. In the presence of culture medium, both the RADA and the functionalized RADA/RGD peptides undergo spontaneous assembly into nanofibers and gelation into stable hydrogels (Fig. 1a). Next, by using TEM, the formation of uniform nanofibers was validated for both types of hydrogels (Fig. 1a and Fig. S3).

To evaluate the stability of the RADA and RADA/RGD hydrogels in culture, the hydrogels were loaded with Y-TSPCs and their diameters were monitored for 7 days. The results demonstrate that both hydrogels do not swell or disrupt in culture medium nor are contracted by the cells, evidenced by no significant changes in diameter over culture time ($p > 0.05$), thus proving their stability and suitability for 3D TSPC cultivation and follow-up investigations (Fig. 1b and c).

3.3. Y- and A-TSPCs survive, proliferate and do not become apoptotic in the nanofiber hydrogels

Live/Dead staining was performed at various time points. At day 1, Y- and A-TSPCs were homogeneously distributed and viable, and showed a round cell shape within both hydrogel types. At day 3 and 7, Y-TSPCs stretched and acquired elongated cell morphology. Strikingly, A-TSPCs, known for their abnormal cell morphology in 2D culture, became very comparable from the Y-TSPCs when cultivated in RADA or RADA/RGD hydrogels. (Fig. 2a, Fig. S4 and Fig. S5). Furthermore, both TSPC types remained viable throughout the whole culture period and only very minor cell fraction was positive for ethidium homodimer-1. Cell viability was additionally confirmed by Resazurin assay (Fig. 2b). After 6 h, A-TSPCs showed lower cell metabolic activity than Y-TSPCs in both hydrogels. Interestingly, A-TSPC recovered after 24 h and reached comparable Resazurin values to Y-TSPC after 72 h (Fig. 2b). However, no significant difference was detected between the Y-TSPC and A-TSPC groups at all observed time points ($p > 0.05$). Furthermore, our JC-1 results clearly demonstrated that neither Y-TSPCs nor A-TSPCs enter apoptosis in both gel types over time (Fig. 2c).

3.4. A-TSPCs acquire Y-TSPC phenotype and properly align in the nanofiber hydrogels

To reveal the cell morphology and cytoskeletal organization, we further examined the TSPCs morphology and F-actin organization in RADA and RADA/RGD hydrogels by evaluating fluorescent phalloidin staining and follow up quantification of cell aspect ratio and cell territory. The results revealed that similar to Y-TSPCs, A-TSPCs were well stretched and displayed a spindle shape in both hydrogels (Fig. 3a). The F-actin organization of A-TSPCs was also normalized and appeared comparable with that of Y-TSPCs (Fig. 3a). Cell aspect ratio calculations revealed comparable values of around 0.2 (cell width/length) for both cell types. A significant difference was reached only between A-TSPC RADA group versus Y-TSPC RADA/RGD group ($p < 0.05$) (Fig. 3b). Regarding cell area, there was no significant difference detected between the Y-TSPCs and A-TSPCs cultured in either of the 3D nanofiber hydrogels ($p > 0.05$) (Fig. 3c). Regarding cell alignment, toluidine blue stainings of semi-thin hydrogel sections and 2D-FFT analyses, further demonstrated that both Y- and A-TSPCs elongate and distribute homogenously, and anisotropically align (Fig. 3d and e).

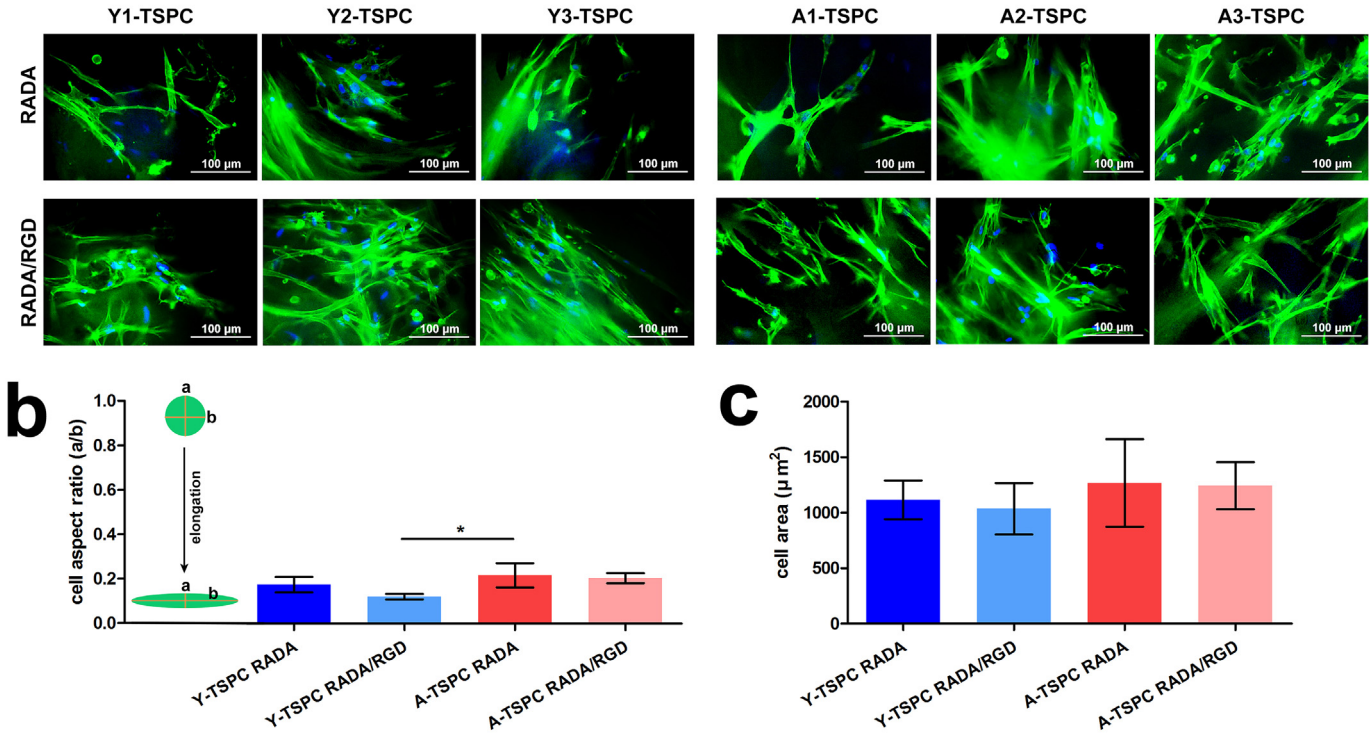

Fig. 3. Analysis of cytoskeletal organization, cell morphology and alignment within the nanofiber hydrogels. (a) Representative images of F-actin staining at day 7 (n = 3 Y-TSPC and n = 3 A-TSPC donors, 2 gels/donor). (b) Quantification of cell aspect ratio (a/b; a, cell width; b, cell length) of Y-TSPCs and A-TSPCs, (for each cell type n = 3 donors, 2 gels/donor, 45 cells/group); $p < 0.05$ (*). (c) Quantification of cell area of Y-TSPCs and A-TSPCs donors (for each cell type n = 3 donors, 2 gels/donor, 45 cells/group). (d) Representative images of toluidine blue stained semi-thin sections of Y- and A- TSPCs (for each cell type n = 3 donors, 1 gel/donor) cultured in the RADA and RADA/RGD peptide hydrogels for 7 days. Double-headed arrows indicate the TSPC orientation. (e) Representative 2D-FFT alignment analyzes of toluidine blue-based images. For each cell type 3 donors, 1 image/donor were analyzed.

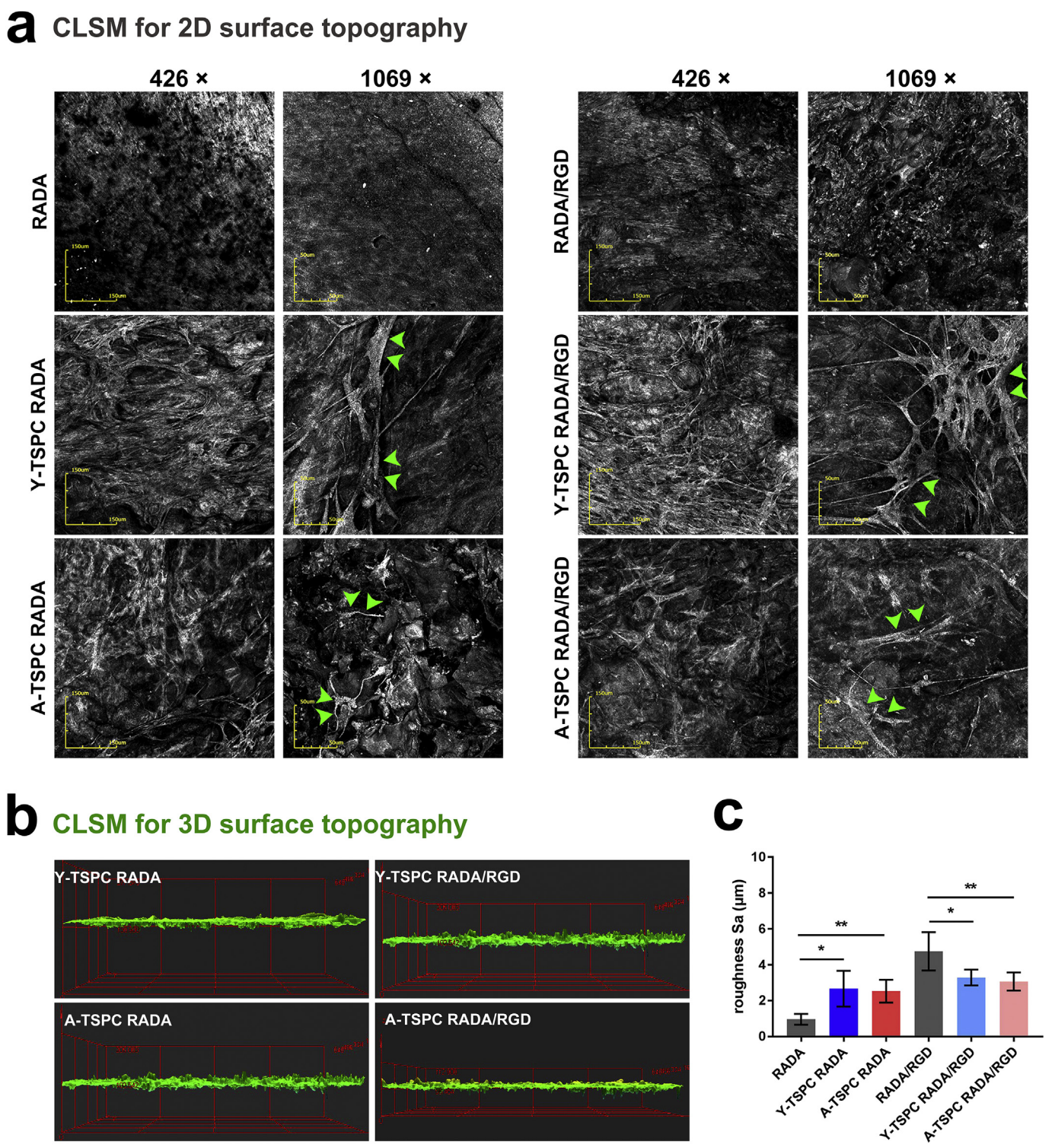

Fig. 4. Confocal laser scanning microscopy (CLSM) and surface topography analysis. (a) Representative top view CLSM images of empty and TSPC-loaded RADA and RADA/RGD nanofiber hydrogels at day 7 of culture (for each cell type n = 3 donors, 1 gel/donor). TSPCs are indicated with green arrow head. (b) Representative side view CLSM (for each cell type n = 3 donors, 1 gel/donor). (c) Calculation of surface rroughness (Sa) of empty and TSPC-loaded hydrogels (for each cell type n = 3 donors, 1 gel/donor, 3 different points/gel analyzed); $p < 0.05$ (*) and $p < 0.01$ (**).

3.5. A-TSPC-loaded nanofiber hydrogels have comparable surface roughness and ultrastructural properties to Y-TSPC controls

Surface properties of the cell-loaded RADA and RADA/RGD nanofiber hydrogels were analyzed by CLSM. The results first revealed that empty RADA hydrogels exhibit more even and flat surface, whilst empty RADA/RGD hydrogel show more grooved and significantly rougher surface (Fig. 4 a and b). After embedding the cells in the hydrogels, Y- and A-TSPCs were clearly visualized on the surface and both cell types appeared elongated with thin and long membranous protrusions (Fig. 4a). Interestingly, both Y- and A-TSPC RADA groups had a significantly higher roughness than the empty RADA group ($p < 0.05$), because of the cells attached onto the surface. In contrast, the Y- and A-TSPC RADA/RGD groups revealed a significantly smoother surface in

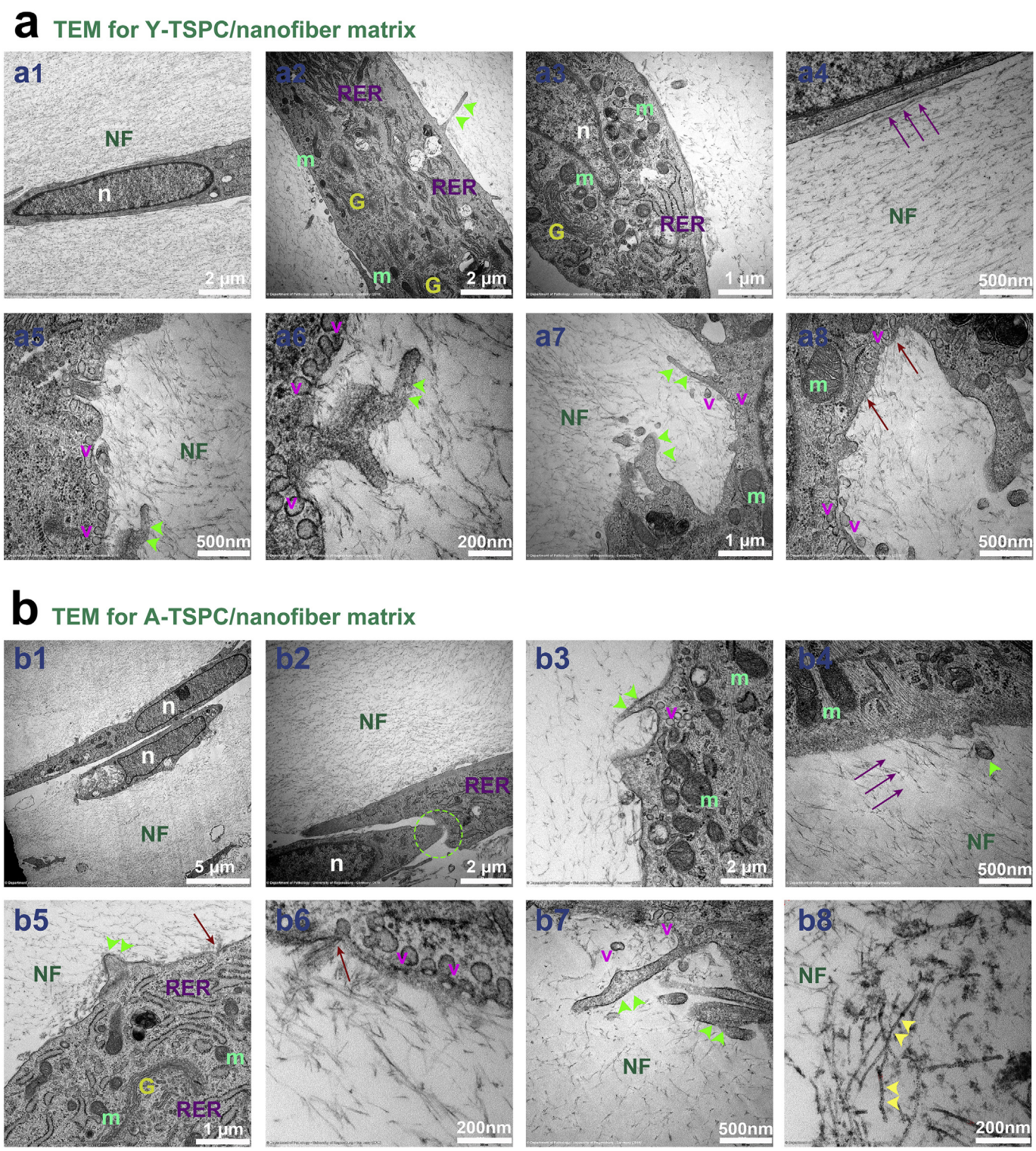

Fig. 5. Transmission electron microscopy (TEM) representative images of Y-TSPCs (a) and A-TSPCs (b) at day 7 of culture. Legend: G, Golgi apparatus; m, mitochondrion; NF, nanofiber; n, nucleus; RER, rough endoplasmic reticulum; v, vesicle; green arrow heads indicate cytoplasmic protrusions and microspikes; purple arrows indicate parallel nanofibers to the cell surface or nanofiber continuum to TSPC cytoskeletal fibers; red arrows indicate nanofiber intake by the TSPCs; yellow arrow heads indicate collagen-like fibers; green circle indicates cell-cell interaction. The TEM results have been conducted with n = 3 Y-TSPC and n = 3 A-TSPC donors, 1 gel/donor.

comparison to the empty RADA/RGD hydrogel, due to the cells filling up the surface grooves ($p < 0.05$) (Fig. 4c). However, there was no significant difference in surface roughness found in between all cell-loaded hydrogel groups ($p > 0.05$) (Fig. 4c). Next, TEM was implemented to study the ultrastructural hydrogel properties and intimate interactions between the cells and the nanofiber matrix (Fig. 5a1-b8 and Fig. S3). Both hydrogels possessed a weakly dense matrix organization, as formed nanofibers were frequently parallel to each other. In addition, a large portion of the nanofibers in RADA/RGD hydrogels appeared shorter than that in the RADA hydrogels (Fig. S3). After

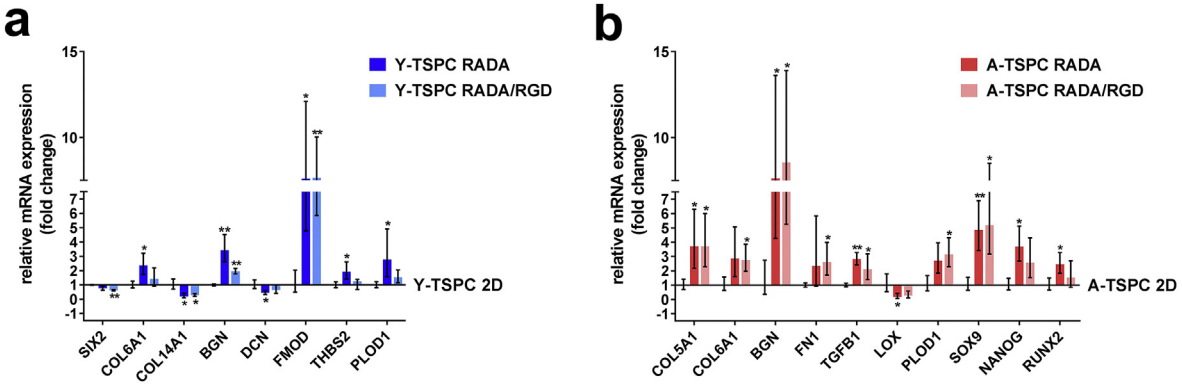

Fig. 6. Gene expression screening of Y-TSPCs (a) and A-TSPCs (b) cultured in 3D nanofiber hydrogels versus classical 2D monolayer by quantitative PCR at day 3. Gene expression was calculated as fold change to the corresponding 2D groups. GAPDH was used as a reference gene. Only genes with significant change in expression are plotted. For full gene list and gene names, refer to Table S1. The qPCR has been conducted with n = 3 Y-TSPC and n = 3 A-TSPC donors, 3 gels/donor; $p < 0.05$ (*) and $p < 0.01$ (**).

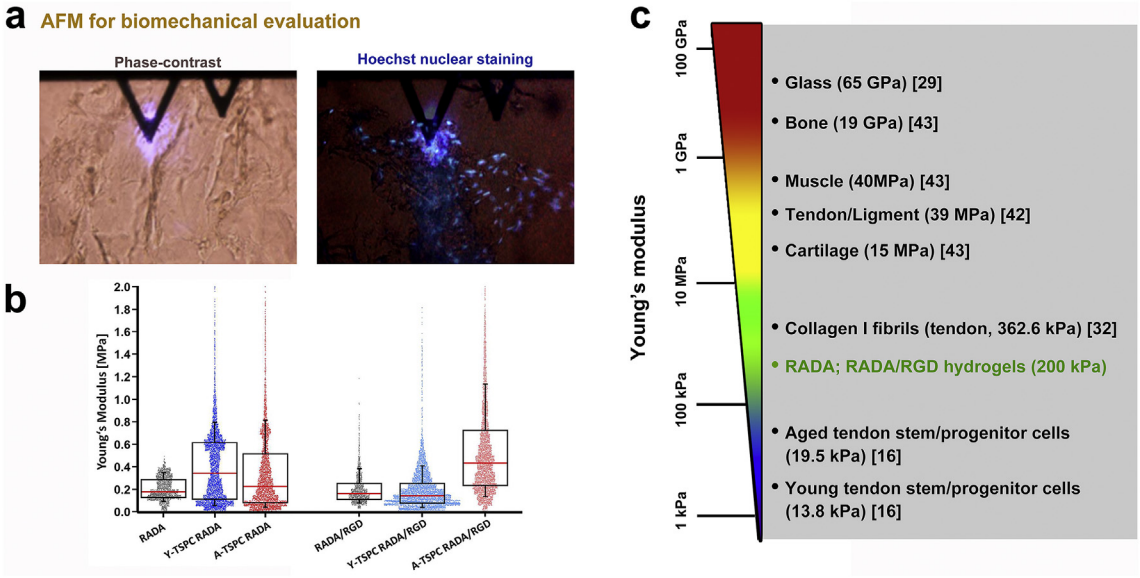

Fig. 7. Force Indentation Atomic Force Microscopy (FI-AFM) at day 7 of culture. (a) Representative phase-contrast and Hoechst nuclear staining imaging used for cantilever positioning. (b) Young's modulus of empty and TSPC-loaded RADA or RADA/RGD nanofiber hydrogels (for each cell type n = 3 donors, 1 gel/donor. For each gel, 625 force curves were analyzed, 1875 force curves per group). (d) Overview of the Young's modulus of different samples related to the musculoskeletal field and the current study on RADA and RADA/RGD nanofiber hydrogels.

cultivation with Y- or A-TSPCs for 7 days, the ECM of both hydrogels became denser, and especially at the periphery of the cells, the nanofibers were well aligned (Fig. 5a1-b7). Interestingly, a continuum between the nanofiber orientation and the TSPC cytoskeletal fibers was observed, as well as the cytoskeletal fibers frequently being assembled in parallel (Fig. 5a4 and b4). Both Y- and A-TSPCs were highly elongated with distinct spindle-like cell shapes (Fig. 5a1,a 2, b1and b2), as well as closely interacting with neighboring cells via cell-cell contacts (Fig. b2) and with the hydrogel ECM via microspikes (slender cytoplasmic protrusions) and double membrane cytoplasmic protrusions (Fig. 5a2, a5-a7, b3-b5 and b7) (Fig. 5). Moreover, numerous mitochondria, and plenty of rough endoplasmic reticulum and Golgi apparatus plus a large number of vesicles were observed in both A- and Y-TSPCs (Fig. 5), indicating high metabolic and secretory activities. Some vesicles were of exocytotic nature, as they were partly fused with the cell membrane and secreted towards the matrix (Fig. 5 a6 and b6). There were also signs of hydrogel matrix intake by the cells (Fig. 5a8, b5 and b6), as well as collagen-like fibers, with characteristic crimp pattern, deposited in the matrix (Fig. 5b8).

3.6. A-TSPCs upregulate tendonogenesis- and multipotency-related gene markers when cultivated in the nanofiber hydrogels and deposite similar amount of type I collagen

Custom-designed quantitative PCR for 48 different genes were designed for validation of tenogenic lineage (tendon-related transcription factors, ECM, collagen and cross-linking genes, other musculoskeletal-, multipotency- and embryonic-related genes and 2 reference genes; Table S1) and experiments were carried out to compare the gene expression of Y- and A-TSPCs in 3D and 2D culture conditions. Differences in gene expression were expressed, as fold change to the corresponding 2D groups and only genes with detected with a significant change in expression are plotted in Fig. 6. First, the obtained data confirmed the expression of major tenogenic genes in both types of TSPCs (Fig. 6 and Fig. S6). Several linage transcription factors showed background levels which is indicative of multipotency. In addition, we conducted analysis of gene expression of A-TSPC to Y-TSPC (set to 1) in 2D (Fig. S6). Our results revealed a tendency of down-regulation of most monitored tenogenic genes, such as COL1, COL3, COL5, COL6, COL14, COL15, EGR1, Eya2, SCX, THSB4, TNC, BGN, FN, NANOG, PLOD1 in the A-

TSPCs in 2D condition compared to Y-TSPCs under corresponding environment. In this situation, only few genes had a tendency of upregulation in the A-TSPCs. However, statistical significant differences were only detected in two genes (TNC and FN) due to (a) larger in-group variance between donors in the Y-TSPC group, and (b) both groups contained n = 3. When cultivated in the 3D nanofiber hydrogels, a large number of genes showed a tendency for upregulation in the 3D A-TSCP groups versus 3D Y-TSPC groups (Fig. S6). Interestingly, 18 genes with significant upregulation or downregulation were found when comparing 3D hydrogel culture conditions to the 2D monolayer controls. For the Y-TSPC RADA and RADA/RGD groups, the tendon-related ECM genes collagen type VI (COL6A1), biglycan (BGN), fibromodulin (FMOD), and thrombospondin 2 (THBS2) and procollagen-lysine 5-dioxygenases (PLOD1) were upregulated ($p < 0.05$), whilst the transcription factor Six homeobox 2 (SIX2), collagen type XIV (COL14A1) and decorin (DCN) were down-regulated in the hydrogels ($p < 0.05$) (Fig. 6a). With respect to A-TSPC RADA and RADAA/RGD groups, collagen type V (COL5A1), collagen type VI (COL6A1), biglycan (BGN), fibronectin 1 (FN1), and transforming growth factor beta 1 (TGFB1) were upregulated ($p < 0.05$). Two collagen cross-linking enzymes exhibited significant differences, namely lysyl oxidase (LOX) was down-regulated in 3D culture ($p < 0.05$), whereas PLOD1 was upregulated in the A-TPSC 3D cultures ($p < 0.05$). Last, the chondrogenic transcription factor, sex determining region Y box 9 (SOX9), the embryonic transcription factor, Nanog homeobox pseudogene 8 (NANOG), and the osteogenic transcription factor, runt-related transcription factor 2 (RUNX2), also showed an upregulation in these conditions ($p < 0.05$) (Fig. 6b). Furthermore, since our previous study [7] has reported A-TSPC secrete significantly less collagen I protein, Y- and A-TSPC-laden RADA hydrogels were collected, cryocut and subjected to collagen I immunofluorescent staining and analysis. This revealed, as in the TEM, comparable collagen I protein deposition by both cell types (Fig. S7, Table S1).

3.7. A-TSPC-loaded hydrogels have comparable Young's modulus to the Y-TSPC controls

FI-AFM was performed to assess the nano-biomechanical properties of empty and cell-loaded RADA and RADA/RGD hydrogels (Fig. 7a). The empty hydrogels showed a similar Young's modulus around 0.2 MPa, which is comparable with the collagen I fibrils in tendon tissue [31] (Fig. 7b and c). After 7 days of TSPC/hydrogel cultivation, both Y- and A-TSPC RADA groups as well as A-TSPC RADA/RGD group showed a tendency to increase their Young's modulus (Fig. 7b). However, multi group analysis did not detect significant differences at this time point ($p > 0.05$).

4. Discussion

TSPC function and fitness is distinctly affected by tendon aging/degeneration, which may lead to declined repair capacity of injured tendons and unsatisfactory clinical outcomes in elderly patients [7,8,12,14,15]. In this study, we explored a rejuvenation strategy for A-TSPCs by providing them with three-dimensional (3D) nanofiber RADA and RADA/RGD hydrogels and comparing their phenotype to that of Y-TSPCs. RADA is an alternating 16-residue peptide and has numerous advantages such as (i) it is made from natural amino acids and degrades into non-toxic products; (ii) it can undergo spontaneous assembly into a nanoscale hydrogel with 10 nm nanofiber diameter and pores of 5–200 nm that offers cells, a true 3D environment similar to the natural extracellular matrix; (iii) its elastic properties are comparable to that of native fibrillar matrices; (iv) it has been shown not to cause inflammatory and immune rejection reactions upon *in vivo* transplantation; and (v) it can be easily further functionalized with various motifs, such as RGD, small molecules or proteins of interest [21–24,32,33].

Based on these advantages, we addressed the question if the nanofiber hydrogels RADA and RADA/RGD would be beneficial for 3D culture of clinically relevant human TSPCs in the context of tendon regeneration.

Comparing Y- to A-TSPCs derived from human Achilles tendon, Kohler et al. [7] observed a profound self-renewal and clonogenic deficits accompanied by earlier entry of A-TSPCs into senescence. Microarray and gene ontology analyses revealed an intriguing transcriptomal shift in A-TSPCs, where most differentially expressed probe sets encoded gene regulating cell-matrix adhesion, migration and actin cytoskeleton. Cytomorphometric and time-lapse analysis confirmed decelerated A-TSPC motion and delayed wound closure concomitant with abnormal cell morphology, high content but slow turnover of actin fibres. Interestingly, A-TSPCs showed augmented expression of the fibronectin-binding integrins α5β1, αvβ3and αvβ5 [34]. Therefore, we involved in the study, the RADA hydrogel variant functionalized with the integrin-binding RGD motif found in fibronectin with the notion that it may better support the A-TSPCs. Our comparative results on the performance of RADA/RGD hydrogel versus RADA hydrogel did not show superior or particular beneficial effects on either of the TSPC types. Possible explanation is that healthy adult tendons contain only low amounts of fibronectin found in the tendon sheets, vascular walls and myotendinous junctions [35,36], thus suggesting that TSPC-fibronectin interaction might not be that critical.

Our present work on cell survival, proliferation, apoptosis and cell morphometry clearly demonstrated that exposure of A-TSPCs to both nanofiber hydrogels results in their rejuvenation to a phenotype similar to that of young donor cells. Furthermore, both Y- and A-TSPCs showed anisotropic alignment enforced by the nanofiber hydrogel matrix. Anisotropy is an important feature of healthy tendon tissues and is closely associated with development, homeostasis and repair [37]. A hallmark of these tissues is their cell alignment along collagen fibers that are orientated parallel to the proximal-distal axis of mechanical extension [38]. In sum, cell behaviour is profoundly affected by the structural and mechanical properties of the surrounding matrix and in particular, we show that TSPCs grow and align in the nanofiber hydrogels in a manner resembling the *in vivo* cell pattern of tendon tissues.

Using CLSM, TEM and IF-AFM technologies were examined in detail the topographic, ultrastructural and elastic properties of the cell-loaded nanofiber hydrogels. Empty RADA and RADA/RGD hydrogels showed different surface roughness caused by the addition of RGD motifs onto the RADA backbone. Interestingly, the surface topography of both hydrogels was changed and also equalized after cultivation with TSPCs. At the ultrastructural level, both types of cells exhibited clear signs of being highly metabolic and secretory, interacting and remodelling the nanofiber matrix. Thus, these findings further confirmed the positive restorative effects of RADA and RADA/RGD hydrogel niche to the A-TSPCs.

As mentioned above, biomechanical attributes of native ECM proteins and biomimetic materials have a great impact onto cell behaviors, and in turn, cells can alter the ECM by remodelling processes [39]. Our novel FI-AFM data reports that the Young's modulus of RADA and RADA/RGD nanofiber hydrogels is comparable to that of collagen I fibrils in tendon tissues [31]. Yet again, TSPCs exerted a clear effect on the nanofiber hydrogel properties; specifically, adding either of the cell types resulted in the increase of the Young's modulus. One reason for this, as shown by TEM, is newly deposited ECM by the TSPCs.

Biomaterials offer a special environment that supports the cells, triggers cell growth, directs their behaviour and can even affect cell fate decision and differentiation [40]. Therefore, we comprehensively analyzed TSPC gene expression profiles in 2D and 3D nanofiber hydrogels conditions. First, our results showed a tendency of down-regulation of most monitored tenogenic genes in the A-TSPCs in 2D condition, compared to Y-TSPCs in the corresponding environment. In this situation, only few genes had a tendency of upregulation in the A-TSPCs. However, statistical significant differences were only detected in two genes, TNC and FN. Statistical significance was not reached due to (a)

larger in-group variance between donors in the Y-TSPC group, and (b) both groups contained n = 3 donors. Follow up investigations should aim to increase the donor cohorts, as well as to design new PCR plates targeting the top dysregulated gene candidates from the microarray data in Kohler et al., 2013 [7] or even to perform RNA sequencing analyses. Interestingly, TNC and FN can bind to each other and can modulate cell adhesion, stretching and shape. Furthermore, both are associated with early development, hence considered "young" gene markers [41,42]. When cultivated in the 3D RADA and RADA/RGD nanofiber hydrogels, a large number of genes showed tendency for upregulation and only two genes were significantly downregulated in the 3D A-TSCP groups versus 3D Y-TSPC groups. Interestingly, several marker genes of tenogenesis and multipotency and even embryogenesis (NANOG) were significantly upregulated in both Y-TSPCs and A-TSPCs, suggesting an additional beneficial effect of the 3D culture. In this study, human TSPCs did not show Tnmd expression neither in 2D not in 3D cultivation. The rapid loss of this marker gene for tendon maturation during *in vitro* human TSPCs expansion has already been described in previous studies [25,31]. One possible way to reconstitute Tnmd expression is in follow up studies to subject the cell-hydrogel composites to biomechanical stimuli, since it is known that Tnmd is a mechanoresponsive gene [25,31].

Since our results indicated that the A-TSPCs exhibit a phenotype comparable to the Y-TSPCs in the 3D nanofiber hydrogels, it is important to confirm that the A-TSPCs were rejuvenated rather than Y-TSPCs beccoming aged. Phase-contrast and F-actin images confirmed that Y-TSPCs convey a classical spindle-like cell shape, whilst A-TSPCs exhibit polygonal cell morphologies with larger cell areas filled up with abundant actin stress fibers. Moreover, additional control experiments, showed that in collagen I hydrogel environment, A-TSPC exhibit 2D polygonal or star-like cell shapes whilst Y-TSPC keep their classical morphology. In addition, resazurin assay showed that the aged cells have significantly declined self-renewal ability in 2D; thus confirming that age-related phenotypic alterations in aged cells persist in 2D. These results are consistent with the findings in Kohler et al., 2013. In this study, type I collagen ELISA data also demonstrated that A-TSPC secrete significantly less amount of this protein but when the cells were cultivated in the RADA hydrogel, they had comparable deposition of collagen I to Y-TSPCs. Altogether, these results support our conclusion that specifically RADA-based nanofiber hydrogels rejuvenates aged cells, rather than ages young cells.

Clinically, the RADA and RADA/RGD nanofiber hydrogels hold great potential, as an injectable cell delivery carrier of TSPCs for boosting tendon repair in both young and elderly patients. In principle, a limitation of hydrogels is to provide complete mechanical restoration in full thickness tendon tears [1,3,4,25]. Nevertheless, hydrogels are attractive materials for enhancing repair of partial tendon lesions, contained tendon defects, or conservatively treated tendon ruptures, as they can be delivered at the site of injury in a minimally invasive manner. In addition, hydrogels can be further enriched by encapsulation of various growth factors or pharmacologics. In order to evaluate the potential of RADA and RADA/RGD hydrogels in tendon regenerative medicine, animal experiments will be carried out in the future by implementing clinically relevant tendon injury models in rodents, which we have recently established [10,43,44].

5. Conclusion

By exposing A-TSPCs to RADA and RADA/RGD 3D nanofiber hydrogels, we developed and report a novel rejuvenation strategy. Both nanofiber hydrogels supported A-TSPC survival, proliferation and alignment in a comparable fashion to Y-TSPCs, as well as restoring their cell morphology and actin organization. Transmission electron, confocal laser scanning and atomic force microscopies demonstrated not only comparable ultrastructural, topographic and biomechanical properties of A- and Y-TSPC-loaded hydrogels but that TSPCs engage in active cross-talk with the nanofiber environment. Lastly, quantitative PCR revealed similar expression profiles, as well as significant upregulation of genes related to tenogenesis and multipotency in both TSPC types. Taken together, the RADA and RADA/RGD nanofiber hydrogels exert a clear rejuvenating effect onto A-TSPCs by offering a specific micro- and nano-niche that possesses certain attributes of native tendon tissues. Thus, by directing cell behaviour, these nanofiber hydrogels hold a potential to overcome specific challenges of cell aging/degeneration, as well as augmenting tendon healing.

Declaration of competing interest

The authors have no conflict of interest to disclose.

Acknowledgments

D.D. acknowledges the EU Twinning Grant Achilles (H2020-WIDESPREAD-05-2017-Twinning Grant Nr. 810850). H.Y. thanks for the support of China Scholarship Council (CSC Grant Nr. 201606200072). S.K. and H.C-S. acknowledge the financial support for CANTER by the Bavarian State Ministry for Science and Education. The authors thank Daniela Drenkard for valuable technical assistance and Dr. Girish Pattappa for English proof-reading.

Appendix A. Supplementary data

Supplementary data to this article can be found online at https://doi.org/10.1016/j.biomaterials.2020.119802.

Date statement

The manuscript includes required protocols in detail and data for reproducibility.

References

[1] D. Docheva, S.A. Muller, M. Majewski, C.H. Evans, Biologics for tendon repair, Adv. Drug Deliv. Rev. 84 (2015) 222–239.
[2] M. Benjamin, E. Kaiser, S. Milz, Structure-function relationships in tendons: a review, J. Anat. 212 (3) (2008) 211–228.
[3] M. Schneider, P. Angele, T.A.H. Jarvinen, D. Docheva, Rescue plan for Achilles: therapeutics steering the fate and functions of stem cells in tendon wound healing, Adv. Drug Deliv. Rev. 129 (2018) 352–375.
[4] Z. Yan, H. Yin, M. Nerlich, C.G. Pfeifer, D. Docheva, Boosting tendon repair: interplay of cells, growth factors and scaffold-free and gel-based carriers, Journal of experimental orthopaedics 5 (1) (2018) 1.
[5] Y. Bi, D. Ehirchiou, T.M. Kilts, C.A. Inkson, M.C. Embree, W. Sonoyama, L. Li, A.I. Leet, B.M. Seo, L. Zhang, S. Shi, M.F. Young, Identification of tendon stem/progenitor cells and the role of the extracellular matrix in their niche, Nat. Med. 13 (10) (2007) 1219–1227.
[6] Y. Li, G. Dai, L. Shi, Y. Lin, M. Chen, G. Li, Y. Rui, The Potential Roles of Tendon Stem/Progenitor Cells in Tendon Ageing, Current stem cell research & therapy, 2018.
[7] J. Kohler, C. Popov, B. Klotz, P. Alberton, W.C. Prall, F. Haasters, S. Muller-Deubert, R. Ebert, L. Klein-Hitpass, F. Jakob, M. Schieker, D. Docheva, Uncovering the cellular and molecular changes in tendon stem/progenitor cells attributed to tendon aging and degeneration, Aging Cell 12 (6) (2013) 988–999.
[8] B. Walia, A.H. Huang, Tendon stem progenitor cells: understanding the biology to inform therapeutic strategies for tendon repair, J. Orthop. Res. Official publication of the Orthopaedic Research Society (2018).
[9] C.H. Lee, F.Y. Lee, S. Tarafder, K. Kao, Y. Jun, G. Yang, J.J. Mao, Harnessing endogenous stem/progenitor cells for tendon regeneration, J. Clin. Investig. 125 (7) (2015) 2690–2701.
[10] D. Lin, P. Alberton, M.D. Caceres, E. Volkmer, M. Schieker, D. Docheva, Tenomodulin is essential for prevention of adipocyte accumulation and fibrovascular scar formation during early tendon healing, Cell Death Dis. 8 (10) (2017) e3116.
[11] F. Wu, M. Nerlich, D. Docheva, Tendon injuries: basic science and new repair proposals, EFORT open reviews 2 (7) (2017) 332–342.
[12] F. Plachel, P. Moroder, R. Gehwolf, H. Tempfer, A. Wagner, A. Auffarth, N. Matis, S. Pauly, M. Tauber, A. Traweger, Risk factors for rotator cuff disease: an experimental study on intact human subscapularis tendons, J. Orthop. Res. : official publication of the Orthopaedic Research Society (2019).
[13] J.E. Ackerman, I. Bah, J.H. Jonason, M.R. Buckley, A.E. Loiselle, Aging does not alter tendon mechanical properties during homeostasis, but does impair flexor

tendon healing, J. Orthop. Res. : official publication of the Orthopaedic Research Society 35 (12) (2017) 2716–2724.
[14] S. Kiderlen, C. Polzer, J.O. Radler, D. Docheva, H. Clausen-Schaumann, S. Sudhop, Age related changes in cell stiffness of tendon stem/progenitor cells and a rejuvenating effect of ROCK-inhibition, Biochem. Biophys. Res. Commun. 509 (3) (2019) 839–844.
[15] C. Popov, J. Kohler, D. Docheva, Activation of EphA4 and EphB2 reverse signaling restores the age-associated reduction of self-renewal, migration, and actin turnover in human tendon stem/progenitor cells, Front. Aging Neurosci. 7 (2015) 246.
[16] A. Birbrair, Stem cell microenvironments and beyond, Adv. Exp. Med. Biol. 1041 (2017) 1–3.
[17] J. Li, K.C. Hansen, Y. Zhang, C. Dong, C.Z. Dinu, M. Dzieciatkowska, M. Pei, Rejuvenation of chondrogenic potential in a young stem cell microenvironment, Biomaterials 35 (2) (2014) 642–653.
[18] B.D. Cosgrove, P.M. Gilbert, E. Porpiglia, F. Mourkioti, S.P. Lee, S.Y. Corbel, M.E. Llewellyn, S.L. Delp, H.M. Blau, Rejuvenation of the muscle stem cell population restores strength to injured aged muscles, Nat. Med. 20 (3) (2014) 255–264.
[19] F. Gelain, D. Bottai, A. Vescovi, S. Zhang, Designer self-assembling peptide nanofiber scaffolds for adult mouse neural stem cell 3-dimensional cultures, PLoS One 1 (2006) e119.
[20] G. Nourissat, F. Berenbaum, D. Duprez, Tendon injury: from biology to tendon repair, Nat. Rev. Rheumatol. 11 (4) (2015) 223–233.
[21] X. Liu, X. Wang, X. Wang, H. Ren, J. He, L. Qiao, F.Z. Cui, Functionalized self-assembling peptide nanofiber hydrogels mimic stem cell niche to control human adipose stem cell behavior in vitro, Acta Biomater. 9 (6) (2013) 6798–6805.
[22] Y. Sun, W. Li, X. Wu, N. Zhang, Y. Zhang, S. Ouyang, X. Song, X. Fang, R. Seeram, W. Xue, L. He, W. Wu, Functional self-assembling peptide nanofiber hydrogels designed for nerve degeneration, ACS Appl. Mater. Interfaces 8 (3) (2016) 2348–2359.
[23] J. Lu, X. Shen, X. Sun, H. Yin, S. Yang, C. Lu, Y. Wang, Y. Liu, Y. Huang, Z. Yang, X. Dong, C. Wang, Q. Guo, L. Zhao, X. Sun, S. Lu, A.G. Mikos, J. Peng, X. Wang, Increased recruitment of endogenous stem cells and chondrogenic differentiation by a composite scaffold containing bone marrow homing peptide for cartilage regeneration, Theranostics 8 (18) (2018) 5039–5058.
[24] E. Genove, C. Shen, S. Zhang, C.E. Semino, The effect of functionalized self-assembling peptide scaffolds on human aortic endothelial cell function, Biomaterials 26 (16) (2005) 3341–3351.
[25] H. Yin, Z. Yan, R.J. Bauer, J. Peng, M. Schieker, M. Nerlich, D. Docheva, Functionalized thermosensitive hydrogel combined with tendon stem/progenitor cells as injectable cell delivery carrier for tendon tissue engineering, Biomed. Mater. 13 (3) (2018) 034107.
[26] R. Tognato, A.R. Armiento, V. Bonfrate, R. Levato, J. Malda, M. Alini, D. Eglin, G. Giancane, T. Serra, A stimuli-responsive nanocomposite for 3D anisotropic cell-guidance and magnetic soft robotics, Adv. Funct. Mater. 29 (9) (2019) 1804647.
[27] C. Prein, N. Warmbold, Z. Farkas, M. Schieker, A. Aszodi, H. Clausen-Schaumann, Structural and mechanical properties of the proliferative zone of the developing murine growth plate cartilage assessed by atomic force microscopy, Matrix biology, Journal of the International Society for Matrix Biology 50 (2016) 1–15.
[28] L.W. Francis, D. Gonzalez, T. Ryder, K. Baer, M. Rees, J.O. White, R.S. Conlan, C.J. Wright, Optimized sample preparation for high-resolution AFM characterization of fixed human cells, J. Microsc. 240 (2) (2010) 111–121.
[29] D. Docheva, D. Padula, C. Popov, W. Mutschler, H. Clausen-Schaumann, M. Schieker, Researching into the cellular shape, volume and elasticity of mesenchymal stem cells, osteoblasts and osteosarcoma cells by atomic force microscopy, J. Cell Mol. Med. 12 (2) (2008) 537–552.
[30] R. Alvarez-Asencio, E. Thormann, M.W. Rutland, Note: determination of torsional spring constant of atomic force microscopy cantilevers: combining normal spring constant and classical beam theory, Rev. Sci. Instrum. 84 (9) (2013) 096102.
[31] S. Dex, P. Alberton, L. Willkomm, T. Sollradl, S. Bago, S. Milz, M. Shakibaei, A. Ignatius, W. Bloch, H. Clausen-Schaumann, C. Shukunami, M. Schieker, D. Docheva, Tenomodulin is required for tendon endurance running and collagen I fibril adaptation to mechanical load, EBioMedicine 20 (2017) 240–254.
[32] J.R. Thonhoff, D.I. Lou, P.M. Jordan, X. Zhao, P. Wu, Compatibility of human fetal neural stem cells with hydrogel biomaterials in vitro, Brain Res. 1187 (2008) 42–51.
[33] M.E. Davis, J.P. Motion, D.A. Narmoneva, T. Takahashi, D. Hakuno, R.D. Kamm, S. Zhang, R.T. Lee, Injectable self-assembling peptide nanofibers create intramyocardial microenvironments for endothelial cells, Circulation 111 (4) (2005) 442–450.
[34] D. Docheva, C. Popov, W. Mutschler, M. Schieker, Human mesenchymal stem cells in contact with their environment: surface characteristics and the integrin system, J. Cell Mol. Med. 11 (1) (2007) 21–38.
[35] M. Lehto, L. Jozsa, M. Kvist, M. Jarvinen, B.J. Balint, A. Reffy, Fibronectin in the ruptured human Achilles tendon and its paratenon. An immunoperoxidase study, Ann. Chir. Gynaecol. 79 (2) (1990) 72–77.
[36] L. Jozsa, M. Lehto, P. Kannus, M. Kvist, A. Reffy, T. Vieno, M. Jarvinen, S. Demel, E. Elek, Fibronectin and laminin in Achilles tendon, Acta Orthop. Scand. 60 (4) (1989) 469–471.
[37] M. Thery, V. Racine, A. Pepin, M. Piel, Y. Chen, J.B. Sibarita, M. Bornens, The extracellular matrix guides the orientation of the cell division axis, Nat. Cell Biol. 7 (10) (2005) 947–953.
[38] J.H. Wang, F. Jia, T.W. Gilbert, S.L. Woo, Cell orientation determines the alignment of cell-produced collagenous matrix, J. Biomech. 36 (1) (2003) 97–102.
[39] N.B. Carrigy, J.P. Carey, A.R. Martin, J.E. Remmers, A. Zareian, Z. Topor, J. Grosse, M. Noga, W.H. Finlay, Simulation of muscle and adipose tissue deformation in the passive human pharynx, Comput. Methods Biomech. Biomed. Eng. 19 (7) (2016) 780–788.
[40] O. Chaudhuri, L. Gu, D. Klumpers, M. Darnell, S.A. Bencherif, J.C. Weaver, N. Huebsch, H.P. Lee, E. Lippens, G.N. Duda, D.J. Mooney, Hydrogels with tunable stress relaxation regulate stem cell fate and activity, Nat. Mater. 15 (3) (2016) 326–334.
[41] K.S. Midwood, M. Chiquet, R.P. Tucker, G. Orend, Tenascin-C at a glance, J. Cell Sci. 129 (23) (2016) 4321–4327.
[42] P. Singh, J.E. Schwarzbauer, Fibronectin and stem cell differentiation - lessons from chondrogenesis, J. Cell Sci. 125 (Pt 16) (2012) 3703–3712.
[43] C.F. Hsieh, P. Alberton, E. Loffredo-Verde, E. Volkmer, M. Pietschmann, P. Muller, M. Schieker, D. Docheva, Scaffold-free Scleraxis-programmed tendon progenitors aid in significantly enhanced repair of full-size Achilles tendon rupture, Nanomedicine 11 (9) (2016) 1153–1167.
[44] C.F. Hsieh, P. Alberton, E. Loffredo-Verde, E. Volkmer, M. Pietschmann, P.E. Muller, M. Schieker, D. Docheva, Periodontal ligament cells as alternative source for cell-based therapy of tendon injuries: in vivo study of full-size Achilles tendon defect in a rat model, Eur. Cells Mater. 32 (2016) 228–240.